



Communication

Nitrogen-Doped Banana Peel-Derived Porous Carbon Foam as Binder-Free Electrode for Supercapacitors

Bingzhi Liu¹, Lili Zhang², Peirong Qi¹, Mingyuan Zhu¹, Gang Wang^{1,3,4}, Yanqing Ma^{1,2,3}, Xuhong Guo^{1,3,4}, Hui Chen¹, Boya Zhang¹, Zhuangzhi Zhao¹, Bin Dai¹ and Feng Yu^{1,3,4,*}

Received: 13 October 2015; Accepted: 11 January 2016; Published: 15 January 2016

Academic Editors: Andy (Xueliang) Sun and Xifei Li

¹ Key Laboratory for Green Processing of Chemical Engineering of Xinjiang Bingtuan, m, Shihezi University, Shihezi 832003, China; bzliushzu@sina.com (B.L.); qpeirong@sina.com (P.Q.); zhumin yuan@shzu.edu.cn (M.Z.); wanggang@shzu.edu.cn (G.W.); mayanqing@shzu.edu.cn (Y.M.); guoxuhong@ecust.edu.cn (X.G.); huichen_@outlook.com (H.C.); boai9594@outlook.com (B.Z.); ezui le@163.com (Z.Z.); daibin_bce@shzu.edu.cn (B.D.)

² Institute of Chemical and Engineering Sciences, Agency for Science, Technology and Research, Jurong Island 627833, Singapore; zhang_lili@ices.a-star.edu.sg

³ Engineering Research Center of Materials-Oriented Chemical Engineering of Xinjiang Production and Construction Corps, Shihezi 832003, China

⁴ Key Laboratory of Materials-Oriented Chemical Engineering of Xinjiang Uygur Autonomous Region, Shihezi 832003, China

* Correspondence: yufeng05@mail.ipc.ac.cn; Tel.: +86-993-205-7272; Fax: +86-993-205-7270

Abstract: Nitrogen-doped banana peel-derived porous carbon foam (N-BPPCF) successfully prepared from banana peels is used as a binder-free electrode for supercapacitors. The N-BPPCF exhibits superior performance including high specific surface areas of 1357.6 m²/g, large pore volume of 0.77 cm³/g, suitable mesopore size distributions around 3.9 nm, and super hydrophilicity with nitrogen-containing functional groups. It can easily be brought into contact with an electrolyte to facilitate electron and ion diffusion. A comparative analysis on the electrochemical properties of BPPCF electrodes is also conducted under similar conditions. The N-BPPCF electrode offers high specific capacitance of 185.8 F/g at 5 mV/s and 210.6 F/g at 0.5 A/g in 6 M KOH aqueous electrolyte *versus* 125.5 F/g at 5 mV/s and 173.1 F/g at 0.5 A/g for the BPPCF electrode. The results indicate that the N-BPPCF is a binder-free electrode that can be used for high performance supercapacitors.

Keywords: banana peel; porous carbon foam; binder free; nitrogen doping; supercapacitor; energy conversion and storage

1. Introduction

Supercapacitors, also known as ultracapacitors or electrochemical capacitors (ECs), have attracted significant attention since the first patent filed in 1957 followed by successful commercialization for hybrid electric vehicles (HEVs) in the 1990s [1]. *Versus* conventional capacitors and Li-ion batteries, supercapacitors offer superior performance including high power capability, good operating voltage, long cycle life (>100,000 cycles), low cost, low maintenance, superior safety, environmentally benign, and fast charge propagation dynamics [2,3]. Recently, supercapacitors have shown advantages over other electrochemical energy storage (EES) devices in many fields requiring high reliability and short load cycle, including portable electronic devices, electric vehicles (EVs), memory back-up systems, *etc.*

Porous carbon along with metal oxides and conductive polymers is the most widely used electrode for supercapacitors because it offers a large surface area, low cost and easy processing [4–6]. Porous carbon offers a high capability for charge separation/accumulation at the electrode/electrolyte

interface, depending on the charge-storage mechanism [7,8]. Generally, porous carbon is derived from organic molecules (e.g., acetonitrile) [9], polymers (e.g., polypyrrole) [10], meta-aminophenol formaldehyde resin [11], monolithic carbide [12], *etc.* This often involves synthetic steps using toxic reagents and complicated synthesis procedures [13]. These concerns as well as requirements for tailored materials have led scientists to develop sustainable, cheap, safe and environmentally friendly porous carbon for use as supercapacitor electrodes.

Here, we report nitrogen-doped banana peel-derived porous carbon foam (N-BPPCF) for use as a binder-free electrode for supercapacitors. The high porosity provided by the framework of the banana peel (BP) offers a high specific surface area and suitable pore size distribution for efficient contact between the electrolytes and the active materials. This, in turn, provides more active sites for electrochemical reactions and outstanding specific capacitance values [14–16]. To the best of our knowledge, this is the first report to describe the use of banana byproducts to generate carbon foam as an electrochemical reagent. This has significant implications for both the chemical and environmental community and is an excellent example of green synthesis.

2. Results and Discussion

To understand the formation mechanism of N-BPPCF, a schematic illustration is proposed in Figure 1a. The pristine BP was firstly air-dried, hydrothermally heated and freeze-dried to yield a brown BP precursor. This precursor has a ribbon pattern-like structure 6 cm long and 2 cm wide, similar to non-processed BP. After the carbonization and nitrogen doping, black N-BPPCF was created with a length of 4.5 cm and a width of 1.5 cm.

Figure 1b,c shows typical scanning electron microscopy (SEM) images of the BPPCF and N-BPPCF porous carbon foam morphology, respectively. We used transmission electron microscopy (TEM) and high-resolution TEM (HRTEM) to further investigate the microstructure details of the BPPCF and N-BPPCF superstructures. Figure 2 shows TEM and HRTEM images at different magnifications of BPPCF and N-BPPCF. Both samples showed a porous structure with a possible pseudographite phase (Figure 2e,f). Moreover, the N-BPPCF produces a high specific surface area (SSA) of $1357.6 \text{ m}^2/\text{g}$, a pore volume of $0.77 \text{ cm}^3/\text{g}$ and a Barrett-Joyner-Halenda (BJH) adsorption average mesopore size distribution around 3.9 nm (Figure 3 and Table 1). This is because the additional NH_3 treatment at $900 \text{ }^\circ\text{C}$ further activates the carbon [17]. The N-BPPCF exhibited higher SSA and bigger pore volume than those of BPPCF. The porous-structured N-BPPCF offers good contact with electrolytes, and these pores strongly favor immediate electron and ion transmission [18].

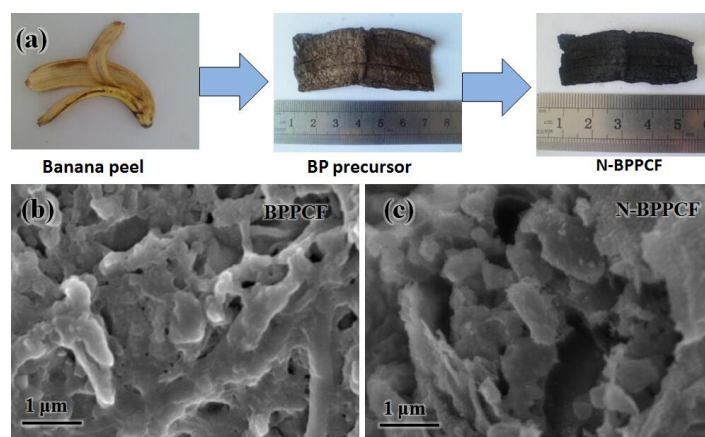


Figure 1. (a) Synthesis of porous carbon foam from banana peels. Scanning electron microscopy (SEM) images of (b) banana peel-derived porous carbon foam (BPPCF) and (c) nitrogen-doped BPPCF (N-BPPCF).

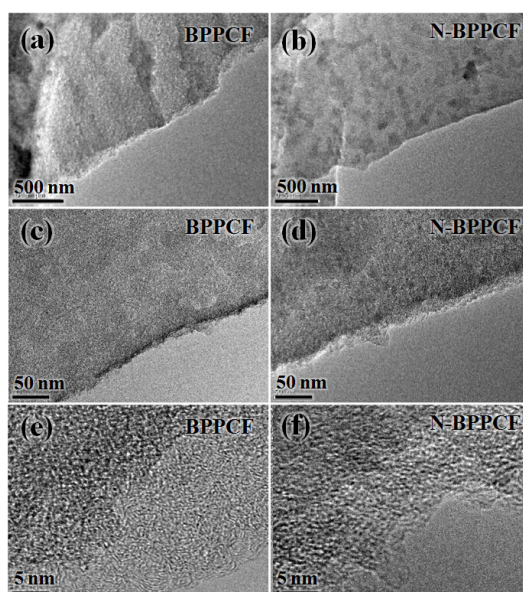


Figure 2. Transmission electron microscopy (TEM) and high-resolution TEM (HRTEM) images at different magnifications of (a, c and e) BPPCF and (b, d and f) N-BPPCF.

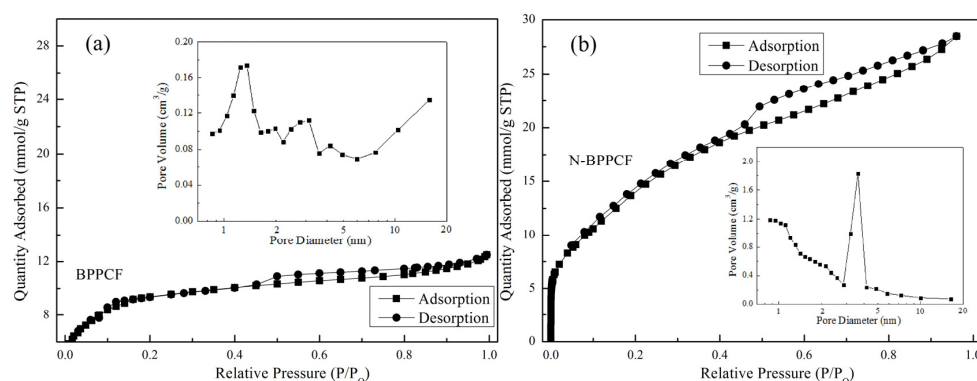


Figure 3. Nitrogen sorption isotherms of (a) BPPCF and (b) N-BPPCF, and the corresponding pore size distribution (insets).

Table 1. Specific surface area, porosity parameters and nitrogen content of the BPPCF and N-BPPCF samples. In the table, S_{BET} stands for BET surface area, while BJH pore diameter, total pore volume and meso-pore volume were abbreviated as D_{BJH} , V_{TPV} and V_{meso} .

Samples	S_{BET} (m^2/g)	D_{BJH} (nm)	V_{TPV} (cm^3/g)	V_{meso} (cm^3/g)
BPPCF	648.3	4.22	0.4183	0.1903
N-BPPCF	1357.6	3.92	0.7651	0.1860

Figure 4a shows the XRD patterns of BPPCF and N-BPPCF. There is a broad peak at 2θ of about 23° corresponding to the (002) plane reflection of graphite. In addition, there is a small shoulder peak that appears at 2θ of 44° which corresponds to the (100) plane reflection of graphite. These two broadening peaks reveal the possible presence of the amorphous phase [19,20] and possible pseudographite nature [21] within the carbonaceous BPPCF and N-BPPCF.

XPS analysis of C, O, and N content in the as-obtained BPPCF and N-BPPCF shows three peaks around 284.2, 288.4 and 444.0 eV, as shown in Figure 4b–d. In the C 1s spectra of the samples, the sharp peak at 284.3 eV corresponds to sp^2 carbon atoms. The peaks at 286.2, 287.5 and 289.2 eV are attributed

to different C–O bonding configurations including C–O, C=O and C–OO bonds which decomposed from BP. Additionally, the peak at 285.1 eV from BPPCF indicates the presence of a C–N bonding configuration degraded mainly from organic compound amino acids in banana peels. Similarly, the bonding configurations of oxygen atoms in samples were characterized by high-resolution O 1s spectra. The O 1s signal consists of three distinct peaks—O=C, O–C and O–N, respectively. The corresponding binding energy of O 1s at 531.1 eV was assigned to O=C, at 532.7 eV to O–C and at 534.4 eV to O–N. All the different oxygen species were formed after thermal annealing of BP. The oxygen content in N-BPPCF decreases slightly with the increase of the nitrogen atomic percentage since the BPPCF was treated by ammonia gas. In the high resolution N 1s spectra, the peak can be attributed to the intensities of four components, such as pyridinic N (397.6 eV), pyrrolic N (399.1 eV), graphitic N (401.0) and pyridine N oxide (402.8 eV). The total nitrogen content in N-BPPCF was 8.7% higher than that of BPPCF (4.2%), as shown in Table 2. In N-BPPCF, pyridinic N constitutes 22.6 at. %, quaternary N constitutes 53.3 at. %, pyrrolic N constitutes 15.3 at. % and pyridine N oxide constitutes 8.8 at. % (Table 3). Due to the doped nitrogen atoms acting as functional groups, the N-BPPCF has good hydrophilicity of the surface and easily contacts with electrolytes [17].

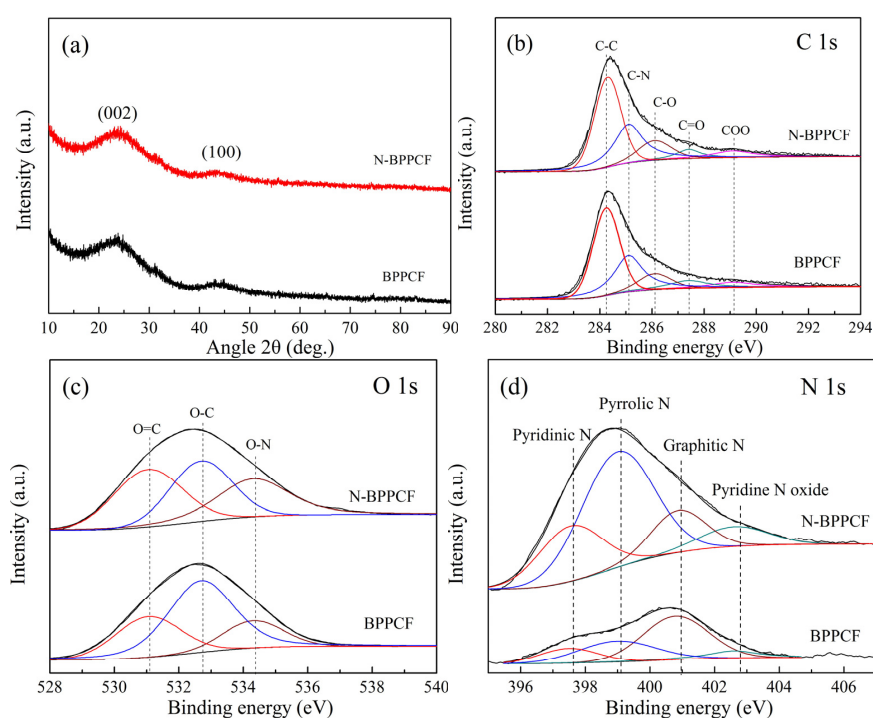


Figure 4. (a) X-ray diffraction (XRD) patterns for BPPCF and N-BPPCF samples. X-ray photoelectron spectroscopy (XPS) spectra of (b) C 1s, (c) O 1s and (d) N 1s for as-obtained BPPCF and N-BPPCF.

Table 2. Element composition by XPS of the BPPCF and N-BPPCF samples.

Samples	C (at. %)	O (at. %)	N (at. %)
BPPCF	90.27	5.52	4.21
N-BPPCF	86.29	5.04	8.67

Table 3. Atomic ratio of various N species from deconvolution N 1s spectra.

Samples	Pyridinic N	Pyrrolic N	Graphitic N	Pyridine N Oxide
BPPCF	14.51	27.35	49.13	9.01
N-BPPCF	22.61	53.27	15.28	8.84

Figure 5 presents cyclic voltammetry (CV) studies used to investigate the electrochemical properties of electrodes. Figure 4c shows CV performance of the BPPCF and N-BPPCF samples in 6 M KOH at the scan rate of 5 mV/s. The CV curves of both samples were rectangular, which is attributed to an ideal capacitance behavior of a porous carbon electrode. The rectangular shape of CV curves is not seriously distorted, even at high scan rates (Figure 5a,b). This indicates the porous carbon is suitable for aqueous electrolytes and that there is little concentration polarization within the pores due to ion transport limitations [22].

The N-BPPCF offers high specific capacitance (185.8 F/g at 5 mV/s) versus 125.5 F/g at 5 mV/s for BPPCF (Figure 5d). With increasing scan rates, the N-BPPCF shows smaller discharge capacitance, such as 179.5 F/g at 10 mV/s, 169.9 F/g at 20 mV/s and 161.9 F/g at 30 mV/s. Even at the scan rate of 40 mV/s and 50 mV/s, the N-BPPCF delivered discharge capacitance of 154.7 F/g and 148.0 F/g, respectively. This is 83.3% and 79.7% of the maximum capacitance at 5 mV/s. It was easy for N-BPPCF to achieve specific capacitance values over 140 F/g—the BPPCF was limited to below 130 F/g. This is principally because the N-BPPCF offers a specific surface area that, in turn, increases the capacitance [8,11,19].

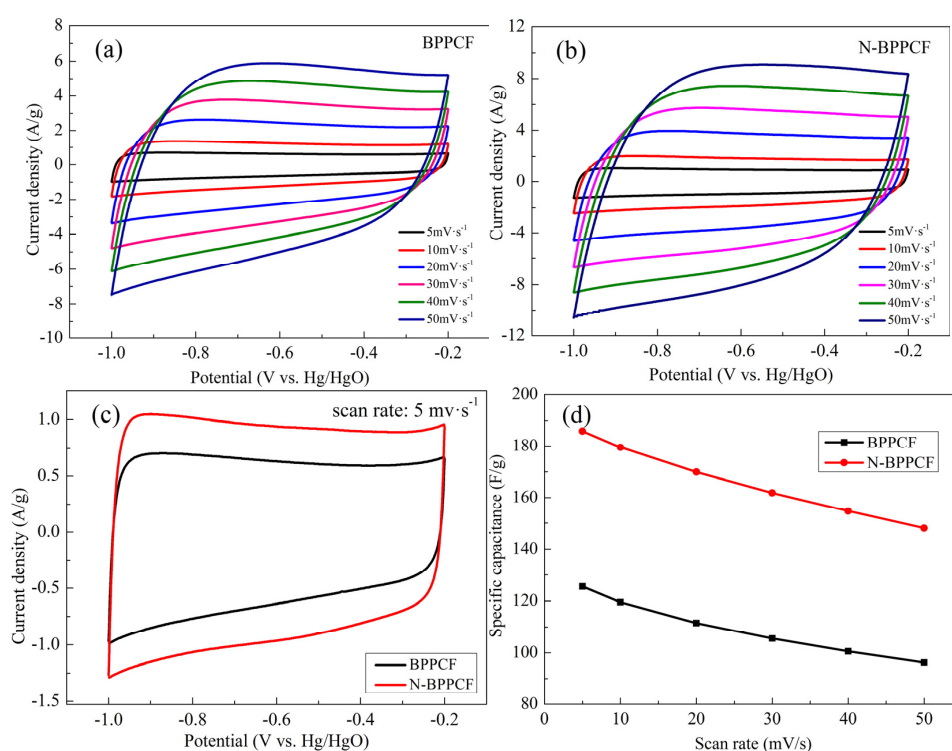


Figure 5. Cyclic voltammogram (CV) curves for (a) BPPCF and (b) N-BPPCF in 6 M KOH at different scan rates. (c) CV curves of the samples at a scan rate of 5 mV/s. (d) Specific capacitance calculated according to CVs.

We used galvanostatic charge/discharge (GCD) measurements to further investigate the electrochemical performance of the BPPCF and N-BPPCF at various current densities (Figure 6). The charge/discharge curves of both samples are linear and symmetrical without any infrared spectroscopy (IR) drop. However, the N-BPPCF offers a high specific capacitance of 210.6 F/g and 178.5 F/g, respectively, at 0.5 A/g and 1.0 A/g, respectively. These are much larger than 173.1 F/g and 136.3 F/g, respectively, for BPPCF. At the current density of 1.5 A/g and 2.0 A/g, the N-BPPCF can still deliver discharge capacitance of 164.3 F/g and 155.0 F/g. This confirms the excellent rate capabilities, with 78.0% and 73.6% of the maximum capacitance (210.6 F/g at 0.5 A/g). Even at the high current density of 2.5 A/g, the discharge capacitance of 146.9 F/g can be achieved. The corresponding obtained capacitance retention of N-BPPCF is 69.8% which is superior to 61.7% of BPPCF (Figure 6d).

All data indicated that the N-BPPCF has great electrochemical performance that is superior to that of BPPCF. Of note, the results are comparable to those reported in literature, such as 175 F/g at 0.5 A/g in 6 M KOH [11] and 212 F/g at 0.5 A/g in 6 M KOH [13].

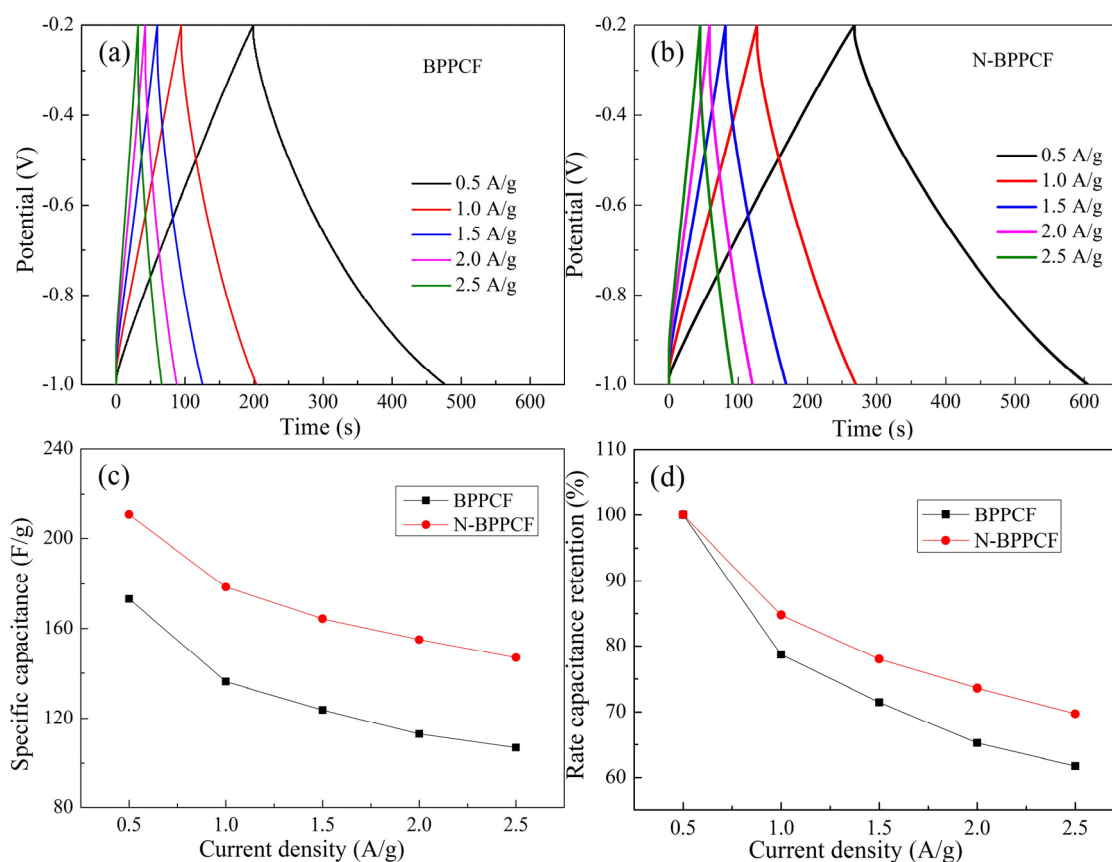


Figure 6. Galvanostatic charge/discharge (GCD) curves for (a) BPPCF and (b) N-BPPCF in 6 M KOH at various current densities. (c) Specific capacitance and (d) the corresponding rate capacitance retention of BPPCF and N-BPPCF.

Figure 7 shows the capacitance of BPPCF and N-BPPCF. Both samples exhibited good reversible capacitance with a capacitance retention rate of about 100% upon cycling and after 500 cycles at 0.5 A/g. Even at 2.5 A/g, N-BPPCF as well as BPPCF performed good cyclic capacitance retention of 100% after 5000 cycles. This underlines the excellent charge–discharge stability of the N-BPPCF as well as BPPCF.

The N-BPPCF architecture offers excellent performance and practical sample preparation for supercapacitors. Of course, bananas are one of most popular fruits worldwide. There are more than 100 million tons produced every year. This results in significant organic waste from the peels. Using this byproduct as an electrode material is both environmentally sensitive and powerful from an electrochemical perspective. This coincides with other work focused on biomass [23] including from bagasse [24], rice husk [25], dead leaves [26], paulownia flower [27], tamarind fruit shell [28], etc.

Furthermore, the as-prepared N-BPPCF has nitrogen-containing functional groups to enhance the capacity, surface wettability and electronic conductivity of carbon materials due to nitrogen doping [29–31]. The N-BPPCF was easily achieved by treating the BPPCF with ammonia to incorporate nitrogen-containing functional groups [32,33]. The as-prepared, binder-free N-BPPCF could be directly used as an electrode without any conductive additives or binders. Recently, interest in binder-free electrodes has grown due to their efficiency and activity [34,35]. We believe that N-BPPCF is a powerful new binder-free electrode for supercapacitors. It has significant potential for use as is or in similar superstructures using other porous carbon foams.

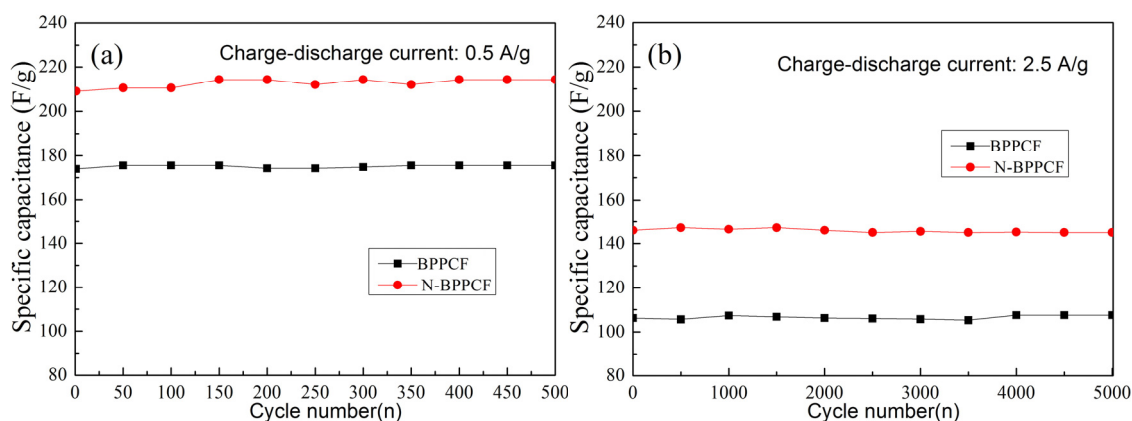


Figure 7. Cycle life of BPPCF and N-BPPCF at various currents: (a) 0.5 A/g for 500 cycles and (b) 2.5 A/g for 5000 cycles.

3. Experimental Section

The raw banana peel (BP) was air-dried, collected and put in a glass dryer prior to use. The air-dried BP (1.5 g) was firstly added into 50 mL deionized water and then transferred into a 100 mL Teflon autoclave and hydrothermally treated at 120 °C for 5 h. Hydrothermal BP was achieved after filtering and washing with deionized water for three times. Subsequently, the as-prepared hydrothermal BP was freeze-dried at −50 °C for 12 h to obtain BP precursor. The carbonization and nitrogen doping process was carried out in two steps. The as-prepared BP precursor was firstly calcined at 900 °C for 5 h in Ar atmosphere to obtain BP-derived porous carbon foam (BPPCF). Secondly, the as-obtained BPPCF was reduced in NH₃ atmosphere at 900 °C for 1 h and then denoted as nitrogen-doped BPPCF (*i.e.*, N-BPPCF).

The BPPCF and N-BPPCF formation mechanism were evaluated with X-ray diffraction (XRD) analysis on a Bruker D8 Advance X-ray diffractometer (Karlsruhe, Germany) with Cu K α radiation ($\lambda = 1.5406 \text{ \AA}$). Scanning electron microscopy (SEM) images were performed on a Hitachi SU8010 microscope (Tokyo, Japan). Transmission electron microscopy (TEM) images were obtained with a Tecnai G2 F30 field emission transmission electron microscope (Hillsboro, OR, USA). Micromeritics ASAP 2020 BEET apparatus (Norcross, GA, USA) was employed to determine Barrett-Joyner-Halenda (BJH) pore structure and Brunauer-Emmett-Teller (BET) specific surface area. The X-ray photoelectron spectroscopy (XPS) data were obtained with an AMICUS/ESCA 3400 electron spectrometer (Manchester, UK) from Kratos Analytical using Mg K α (20 mA 12 KV) radiation. The binding energies were referenced to the C 1s line at 284.8 eV from adventitious carbon.

The electrochemical performance of the as-obtained BPPCF and N-BPPCF was evaluated using a standard three-electrode cell. The electrochemical performance such as cyclic voltammetry (CV) and galvanostatic charge/discharge (GCD) curves were performed using a CHI 660E electrochemical workstation at ambient condition. To fabricate the working electrode in three-electrode configuration, the as-obtained samples were cut into squares with edge length of 10.0 mm. A platinum sheet (10.0 mm \times 10.0 mm) and a Hg/HgO electrode was the counter electrode and the reference electrode, respectively. The potentials were reported relative to the Hg/HgO reference electrode and the electrochemical measurements of the electrodes were recorded after stabilization. CV measurements were carried out at ambient temperature using 6 M KOH aqueous solution as electrolyte, the potential scan rates ranged from 0.5 to 50 mV/s within a potential range of −0.2 to 1.0 V *vs.* Hg/HgO.

The specific capacitances of the electrodes can be calculated by using Equation (1) with the measured CVs and Equation (2) from the galvanostatic discharge branches, respectively [3,36].

$$C = \frac{\int IdV}{v \times \Delta V \times m} \quad (1)$$

Here, C is the gravimetric specific capacitance (F/g), I is the current (A), v is the scan rate (mV/s), ΔV is the potential (V) and m is the total mass (g) of the samples.

$$C = \frac{I \times t}{\Delta V \times m} \quad (2)$$

Here, C is the gravimetric specific capacitance (F/g), I is the discharge current (A), ΔV is the potential (V), m is the total mass (g) of the samples, and t is the discharge time (s).

4. Conclusions

In conclusion, nitrogen-doped banana peel-derived porous carbon foam (N-BPPCF) was successfully prepared and used as a binder-free electrode for supercapacitors. The N-BPPCF shows excellent electrochemical performances including a high specific capacitance of 185.8 F/g at 5 mV/s using CV measurement and 210.6 F/g at 0.5 A/g using galvanostatic charge/discharge measurement. We hope that N-BPPCF architecture will offer an additional way to prepare the binder-free electrodes and it shows potential for the synthesis of many other porous carbon foams.

Acknowledgments: We would like to thank Shishan Sheng (Dalian Institute of Chemical Physics, Chinese Academy of Sciences) for his helpful discussions about XPS analysis. This work was financially supported by the Doctor Foundation of Bingtuan (No. 2014BB004), the National Natural Science Foundation of China (No. 21263021, U1303291) and the Program of Science and Technology Innovation Team in Bingtuan (No. 2015BD003).

Author Contributions: B.D. and F.Y. designed and administered the experiments. B.Z.L., Q.R.Q. and F.Y. performed the experiments. H.C., B.Y.Z. and Z.Z.Z. collected data. L.L.Z., M.Y.Z., G.W., Y.Q.M. and X.H.G. gave technical support. L.L.Z., B.D. and F.Y. gave conceptual advice. All authors contributed to the analysis and discussion of the data and writing the manuscript.

Conflicts of Interest: The authors declare no conflict of interest.

References

1. Wang, G.P.; Zhang, L.; Zhang, J.J. A review of electrode materials for electrochemical supercapacitors. *Chem. Soc. Rev.* **2012**, *41*, 797–828. [[CrossRef](#)] [[PubMed](#)]
2. Zhang, L.L.; Zhou, R.; Zhao, X.S. Graphene-based materials as supercapacitor electrodes. *J. Mater. Chem.* **2010**, *20*, 5983–5992. [[CrossRef](#)]
3. Zheng, C.; Zhou, X.F.; Cao, H.L.; Wang, G.H.; Liu, Z.P. Synthesis of porous graphene/activated carbon composite with high packing density and large specific surface area for supercapacitor electrode material. *J. Power Sources* **2014**, *258*, 290–296. [[CrossRef](#)]
4. Zhang, Y.; Feng, H.; Wu, X.; Wang, L.; Zhang, A.; Xia, T.; Dong, H.; Li, X.; Zhang, L. Progress of electrochemical capacitor electrode materials: A review. *Int. J. Hydrog. Energy* **2009**, *34*, 4889–4899. [[CrossRef](#)]
5. Bose, S.; Kuila, T.; Mishra, A.K.; Rajasekar, R.; Kim, N.H.; Lee, J.H. Carbon-based nanostructured materials and their composites as supercapacitor electrodes. *J. Mater. Chem.* **2012**, *22*, 767–784. [[CrossRef](#)]
6. Campagnol, N.; Romero-Vara, R.; Deleu, W.; Stappers, L.; Binnemans, K.; de Vos, D.E.; Franssaer, J. A Hybrid Supercapacitor Based on Porous Carbon and the Metal-Organic Framework MIL-100(Fe). *Chemelectrochem* **2014**, *1*, 1182–1188. [[CrossRef](#)]
7. Merlet, C.; Rotenberg, B.; Madden, P.A.; Taberna, P.L.; Simon, P.; Gogotsi, Y.; Salanne, M. On the molecular origin of supercapacitance in nanoporous carbon electrodes. *Nat. Mater.* **2012**, *11*, 306–310. [[CrossRef](#)] [[PubMed](#)]
8. Yuan, C.Z.; Gao, B.; Shen, L.F.; Yang, S.D.; Hao, L.; Lu, X.J.; Zhang, F.; Zhang, L.J.; Zhang, X.G. Hierarchically structured carbon-based composites: Design, synthesis and their application in electrochemical capacitors. *Nanoscale* **2011**, *3*, 529–545. [[CrossRef](#)] [[PubMed](#)]
9. Xia, Y.D.; Mokaya, R. Generalized and facile synthesis approach to N-doped highly graphitic mesoporous carbon materials. *Chem. Mater.* **2005**, *17*, 1553–1560. [[CrossRef](#)]
10. Su, F.B.; Poh, C.K.; Chen, J.S.; Xu, G.W.; Wang, D.; Li, Q.; Lin, J.Y.; Lou, X.W. Nitrogen-containing microporous carbon nanospheres with improved capacitive properties. *Energy Environ. Sci.* **2011**, *4*, 717–724. [[CrossRef](#)]

11. Zhou, J.; Zhang, Z.S.; Xing, W.; Yu, J.; Han, G.X.; Si, W.J.; Zhuo, S.P. Nitrogen-doped hierarchical porous carbon materials prepared from meta-aminophenol formaldehyde resin for supercapacitor with high rate performance. *Electrochim. Acta* **2015**, *153*, 68–75. [[CrossRef](#)]
12. Chmiola, J.; Largeot, C.; Taberna, P.L.; Simon, P.; Gogotsi, Y. Monolithic Carbide-Derived Carbon Films for Micro-Supercapacitors. *Science* **2010**, *328*, 480–483. [[CrossRef](#)] [[PubMed](#)]
13. He, C.L.; Liu, Y.L.; Xue, Z.P.; Zheng, M.T.; Wang, H.B.; Xiao, Y.; Dong, H.W.; Zhang, H.R.; Lei, B.F. Simple Synthesis of Carboxylate-Rich Porous Carbon Microspheres for High-Performance Supercapacitor Electrode Materials. *Int. J. Electrochem. Sci.* **2013**, *8*, 7088–7098.
14. Seo, D.H.; Han, Z.J.; Kumar, S.; Ostrikov, K. Structure-Controlled, Vertical Graphene-Based, Binder-Free Electrodes from Plasma-Reformed Butter Enhance Supercapacitor Performance. *Adv. Energy Mater.* **2013**, *3*, 1316–1323. [[CrossRef](#)]
15. Yu, F.; Ge, S.G.; Li, B.; Sun, G.Z.; Mei, R.G.; Zheng, L.X. Three-Dimensional Porous LiFePO₄: Design, Architectures and High Performance for Lithium Ion Batteries. *Curr. Inorg. Chem.* **2012**, *2*, 194–212. [[CrossRef](#)]
16. Yu, F.; Zhang, L.; Li, Y.; An, Y.; Zhu, M.; Dai, B. Mechanism studies of LiFePO₄ cathode material: Lithiation/delithiation process, electrochemical modification and synthetic reaction. *RSC Adv.* **2014**, *4*, 54576–54602. [[CrossRef](#)]
17. Horikawa, T.; Sakao, N.; Sekida, T.; Hayashi, J.; Do, D.D.; Katoh, M. Preparation of nitrogen-doped porous carbon by ammonia gas treatment and the effects of N-doping on water adsorption. *Carbon* **2012**, *50*, 1833–1842. [[CrossRef](#)]
18. Wang, D.W.; Li, F.; Liu, M.; Lu, G.Q.; Cheng, H.M. 3D aperiodic hierarchical porous graphitic carbon material for high-rate electrochemical capacitive energy storage. *Angew. Chem. Int. Edit.* **2008**, *47*, 373–376. [[CrossRef](#)] [[PubMed](#)]
19. Subramanian, V.; Luo, C.; Stephan, A.M.; Nahm, K.S.; Thomas, S.; Wei, B.Q. Supercapacitors from activated carbon derived from banana fibers. *J. Phys. Chem. C* **2007**, *111*, 7527–7531. [[CrossRef](#)]
20. Lv, Y.K.; Gan, L.H.; Liu, M.X.; Xiong, W.; Xu, Z.J.; Zhu, D.Z.; Wright, D.S. A self-template synthesis of hierarchical porous carbon foams based on banana peel for supercapacitor electrodes. *J. Power Sources* **2012**, *209*, 152–157. [[CrossRef](#)]
21. Lotfabad, E.M.; Ding, J.; Cui, K.; Kohandehghan, A.; Kalisvaart, W.P.; Hazelton, M.; Mitlin, D. High-Density Sodium and Lithium Ion Battery Anodes from Banana Peels. *Acs Nano* **2014**, *8*, 7115–7129. [[CrossRef](#)] [[PubMed](#)]
22. Qie, L.; Chen, W.M.; Xu, H.H.; Xiong, X.Q.; Jiang, Y.; Zou, F.; Hu, X.L.; Xin, Y.; Zhang, Z.L.; Huang, Y.H. Synthesis of functionalized 3D hierarchical porous carbon for high-performance supercapacitors. *Energy Environ. Sci.* **2013**, *6*, 2497–2504. [[CrossRef](#)]
23. Titirici, M.M.; White, R.J.; Brun, N.; Budarin, V.L.; Su, D.S.; del Monte, F.; Clark, J.H.; MacLachlan, M.J. Sustainable carbon materials. *Chem. Soc. Rev.* **2015**, *44*, 250–290. [[CrossRef](#)] [[PubMed](#)]
24. Hao, P.; Zhao, Z.H.; Tian, J.; Li, H.D.; Sang, Y.H.; Yu, G.W.; Cai, H.Q.; Liu, H.; Wong, C.P.; Umar, A. Hierarchical porous carbon aerogel derived from bagasse for high performance supercapacitor electrode. *Nanoscale* **2014**, *6*, 12120–12129. [[CrossRef](#)] [[PubMed](#)]
25. Gao, Y.; Li, L.; Jin, Y.M.; Wang, Y.; Yuan, C.J.; Wei, Y.J.; Chen, G.; Ge, J.J.; Lu, H.Y. Porous carbon made from rice husk as electrode material for electrochemical double layer capacitor. *Appl. Energy* **2015**, *153*, 41–47. [[CrossRef](#)]
26. Senthilkumar, S.T.; Selvan, R.K. Flexible Fiber Supercapacitor Using Biowaste-Derived Porous Carbon. *Chemelectrochem* **2015**, *2*, 1111–1116. [[CrossRef](#)]
27. Chang, J.L.; Gao, Z.Y.; Wang, X.R.; Wu, D.P.; Xu, F.; Wang, X.; Guo, Y.M.; Jiang, K. Activated porous carbon prepared from paulownia flower for high performance supercapacitor electrodes. *Electrochim. Acta* **2015**, *157*, 290–298. [[CrossRef](#)]
28. Senthilkumar, S.T.; Selvan, R.K.; Melo, J.S.; Sanjeeviraja, C. High Performance Solid-State Electric Double Layer Capacitor from Redox Mediated Gel Polymer Electrolyte and Renewable Tamarind Fruit Shell Derived Porous Carbon. *ACS Appl. Mater. Inter.* **2013**, *5*, 10541–10550. [[CrossRef](#)] [[PubMed](#)]
29. Chen, L.F.; Zhang, X.D.; Liang, H.W.; Kong, M.G.; Guan, Q.F.; Chen, P.; Wu, Z.Y.; Yu, S.H. Synthesis of Nitrogen-Doped Porous Carbon Nanofibers as an Efficient Electrode Material for Supercapacitors. *ACS Nano* **2012**, *6*, 7092–7102. [[CrossRef](#)] [[PubMed](#)]

30. Sun, K.J.; Feng, E.K.; Peng, H.; Ma, G.F.; Wu, Y.J.; Wang, H.P.; Lei, Z.Q. A simple and high-performance supercapacitor based on nitrogen-doped porous carbon in redox-mediated sodium molybdate electrolyte. *Electrochim. Acta* **2015**, *158*, 361–367. [[CrossRef](#)]
31. Lee, M.; Kim, G.P.; Song, H.D.; Park, S.; Yi, J. Preparation of energy storage material derived from a used cigarette filter for a supercapacitor electrode. *Nanotechnology* **2014**, *25*. [[CrossRef](#)] [[PubMed](#)]
32. Zhao, L.; Fan, L.Z.; Zhou, M.Q.; Guan, H.; Qiao, S.Y.; Antonietti, M.; Titirici, M.M. Nitrogen-Containing Hydrothermal Carbons with Superior Performance in Supercapacitors. *Adv. Mater.* **2010**, *22*, 5202–5206. [[CrossRef](#)] [[PubMed](#)]
33. Shiraishi, S. Heat-treatment and Nitrogen-doping of Activated Carbons for High Voltage Operation of Electric Double Layer Capacitor. *Key Eng. Mater.* **2012**, *497*, 80–86. [[CrossRef](#)]
34. Zhu, G.Y.; He, Z.; Chen, J.; Zhao, J.; Feng, X.M.; Ma, Y.W.; Fan, Q.L.; Wang, L.H.; Huang, W. Highly conductive three-dimensional MnO₂-carbon nanotube-graphene-Ni hybrid foam as a binder-free supercapacitor electrode. *Nanoscale* **2014**, *6*, 1079–1085. [[CrossRef](#)] [[PubMed](#)]
35. Liu, W.W.; Lu, C.X.; Wang, X.L.; Liang, K.; Tay, B.K. *In situ* fabrication of three-dimensional, ultrathin graphite/carbon nanotube/NiO composite as binder-free electrode for high-performance energy storage. *J. Mater. Chem. A* **2015**, *3*, 624–633. [[CrossRef](#)]
36. Li, H.L.; Jiang, L.X.; Cheng, Q.L.; He, Y.; Pavlinek, V.; Saha, P.; Li, C.Z. MnO₂ nanoflakes/hierarchical porous carbon nanocomposites for high-performance supercapacitor electrodes. *Electrochim. Acta* **2015**, *164*, 252–259. [[CrossRef](#)]



© 2016 by the authors; licensee MDPI, Basel, Switzerland. This article is an open access article distributed under the terms and conditions of the Creative Commons by Attribution (CC-BY) license (<http://creativecommons.org/licenses/by/4.0/>).